Time-dependent Measurement of Charge Density on the Bottom of High Aspect Capillary Hole in Pulse-Modulated VHF Capacitively Coupled Ar Plasma

Makoto Moriyama,[1] Naoya Nakahara,[1] Kazuaki Kurihara,[2] Daiki Iino,[2] Hiroyuki Fukumizu,[2] Haruka Suzuki[1,3] and Hirotaka Toyoda[1,3,4]

[1]*Department of Electronics, Nagoya University, Furo-cho, Chikusa-ku, Nagoya 464-8603, Japan*

[2]*Institute of Memory Technology Research & Development, Kioxia Corp. Isogo-ku Yokohama, 235-0017, Japan*

[3]*Center for Low Temperature Plasma Sciences, Nagoya University, Furo-cho, Chikusa-ku, Nagoya 464-8603, Japan*

[4]*National Institute for Fusion Science, 322-6, Oroshi, Toki, 509-5292 Japan.*

Abstract

Charging and discharging behavior of high aspect-ratio hole capillary plate (CP) exposed to a pulse-modulated very high frequency (VHF) capacitively-coupled plasma is investigated. From an equivalent circuit model, time-dependent charge density on the bottom of the CP is quantitatively evaluated. Aspect ratio of the CP plays very important role for the charging current, although the discharge current is dominated by the leakage current of the CP. Importance of electron current flowing into the CP bottom during the VHF pulse-on phase is suggested at higher self-bias voltages.

Keywords:

high-aspect hole, charge-up, VHF plasma, pulse-modulated plasma, charging current

1. Introduction

Anisotropic etching is indispensable in fabrication of nanoscale or three-dimensional semiconductor devices. To realize fine or high-aspect-ratio patterns, a precise control of etching process at the nanometer scale is required. It is well known that anisotropic etching proceeds by surface chemical reactions with neutral radical species transported from plasma onto the substrate, as well as highly energetic ion bombardments accelerated by negative electric field in the sheath. To achieve a precise etching with high throughput, accurate control of the surface reaction based on a critical balance of amounts and energies of the ions and neutral species is required. As one of the solutions, in the 1990s dual-frequency capacitively-coupled plasma (CCP) sources was introduced wherein high-density plasma and high-bias voltage is realized by a combination of very high frequency (VHF) and low frequency (LF) power to control the plasma density and the bias voltage, respectively.[1,2] This combination enables the functional separation of the plasma density and the ion impingement energy. The dual frequency plasmas (DFPs) have extensively been studied from the viewpoints of theory, [3] experiments, [4] and simulations. [5,6]

Apart from the studies of plasma sources, feature control of etching holes has also been intensively studied.[7-11] Charge-up of etching holes or trenches is also an important issue, as the charge on the surface distorts the trajectory of the ions and reduces the etching rate, leading to feature degradation. Undesired profiles such as bowing and etch stops are caused by the charging effects.

In the actual etching process, it has been found that the charge-up behavior depends on the etching material. For example, studies on the etching characteristics of open patterned and narrow patterned edges of conductive polysilicon have shown pattern-dependent charge-up behavior through experiments[12,13] and simulations[14-17]. Charge-up behavior in dielectric etch holes has been widely studied along with the effect of charge accumulation on the etching rate[18]. Furthermore, the electrical conductivity of fluorocarbon films formed on the sidewalls of the etch holes has also been studied.[19-21]

A charge-up suppression method using neutral beams has been proposed[22,23] and the charge-up behavior on the etching feature has been clarified using simulations.[24,25] Charge cancellation in etching holes or trenches is required to minimize the deformation of the etching feature. For this purpose, the use of electron beams[26] and negative ions[27,28] to cancel the accumulated charge has been investigated. Among the various techniques for suppressing hole-bottom charge-up, pulsed-operation of the plasma source[18, 29-31] is currently considered to be useful in the actual etching processes. Given the recent development of high-density plasma sources, the elucidation of VHF plasma sources by pulsed operation could have important implications for future high-aspect ratio (HAR) etching processes.

Experimental studies on the charge-up behavior at the bottom of the etching hole have been carried out by several researchers. Kurihara et al. investigated fluorocarbon CCP at 13.56 MHz and measured fluorocarbon ions passing through the capillary plate (CP) as a model for etching holes on

a powered electrode. They tested a commercially available plate having small HAR holes and a specially made CP using a mass spectrometer with an energy analyzer. [32] Ohtake et al. reported voltage fluctuations at the bottom of the specially made capillary plate in 13.56 MHz pulsed inductively coupled plasma (ICP).[33] Negishi et al. investigated the charge-up at the bottom of a microchannel plate (MCP) (AR:<20) in a 200 MHz electron cyclotron resonance (ECR) plasma.[34] These studies showed the behavior of ions and charge-up at the bottom of real-scale or real AR holes and provided important information on the performance of the HAR hole bottom in response to charge-up. However, to the best of our knowledge, no study has reported the absolute values of the charge-density at the bottom and top of the HAR hole. Moreover, no study has yet reported the temporal variations in charge densities at the top and bottom of the HAR hole in a pulsed operation plasma.

So far, we have investigated charging-up process on the bottom of the CP. We have developed a method for quantitative measurement of the charge density on the CP bottom, based on an equivalent circuit model and measurement of the voltage on the bottom of the CP.[35] In this study, we report time-dependent charge density on the CP bottom with different aspect ratios from 12 to 50. Charging and discharging properties of the CP bottom charge is discussed.

2. Experimental setup

Experimental apparatus has been reported in a previous paper[35] and is not

shown here. A vacuum vessel of 16 cm in diameter and 18 cm in height is evacuated by a turbomolecular pump. A powered electrode and a grounded electrode with the same diameter of 11 cm and an electrode distance of 3 cm are placed on the bottom and top of the vessel, respectively. The bottom electrode is covered with an alumina plate of 0.5 mm in thickness. Pure Ar gas is introduced to the vessel from the grounded electrode at a flow rate of 30 sccm. Pressure is kept at 2 Pa by a conductance valve. Pulse-modulated 40 MHz VHF power (peak power: <600 W, pulse frequency: 1 kHz, duty cycle: 50%) is applied to a powered electrode on the bottom of a cylindrical vessel. Typical plasma density, electron temperature and plasma potential are $2x10^{17}$ m^{-3}, ~3 eV and ~30 V, respectively, at Ar pressure of 4 Pa and VHF power of 300 W.

Figure 1 shows schematic set-up of the capillary plate (CP). CPs with aspect-ratios (ARs) of 12, 30 or 50, which correspond to hole diameters of 25, 10 and 6 μm, respectively, is placed on the alumina-covered powered electrode. CP diameter (2.5 cm), thickness (0.3 mm) and hole opening ratio (60%) of different ARs are the same. On the bottom of the CP, an electrode for the voltage measurement is placed. A wire is connected to the CP bottom electrode and voltage of the CP bottom electrode is measured by a high voltage probe (HVP) with an input resistance of 100 MΩ and an input capacitance of 3 pF. To obtain flat frequency dependence of the HVP measurement, the HVP is precisely calibrated taking account for stray capacitances of vacuum feed through.

Charge density on the CP bottom electrode is evaluated by a

procedure which has been described in our previous work.[35] Briefly, VHF peak-to-peak voltage on the top of the CP (V_{PP}^{TOP}) is evaluated using peak-to-peak voltage on the CP bottom electrode (V_{PP}^{BTM}). In this evaluation, the alumina plate and the CP are modeled as capacitances. Next, V_{AVE}^{TOP}, *i.e.*, self-bias voltage on the CP top, is obtained from the estimated V_{PP}^{TOP}. In this procedure, relation between the V_{PP}^{TOP} and the V_{AVE}^{TOP} has been measured beforehand. From measured V_{AVE}^{TOP}, V_{AVE}^{BTM}, effective CP capacitance, and alumina capacitance, surface charge density on the CP bottom is evaluated.

3. Results and Discussions

Figure 2 shows typical voltage waveform on the bottom of the CP. Aspect ratio of the CP is 30 and VHF power is 200 W. Here, t=0 and 0.5 ms are defined as the timing when the pulse VHF power is turned-on and -off, respectively. During the VHF power is on, 40 MHz oscillation at maximum and minimum VHF voltages of +193 V and -115 V are observed. When the VHF power is off, the 40 MHz oscillation disappears and the bottom voltage increases up to ~120 V due to relaxation of negative charge on the CP top. Figure 3 shows average voltages of the CP top and bottom, evaluated from the result of Fig. 2, using the evaluation scheme of our previous work.[35] The V_{AVE}^{TOP} is negatively biased during the VHF power is on and is ~10 V during the VHF power is off. The V_{AVE}^{BTM} is always higher than the V_{AVE}^{TOP} both in the cases of the VHF power is on and off. Similar time dependences of the CP top and bottom voltages indicate that the CP bottom voltage is

influenced by the electric field induced by the CP top voltage. The positive shift of the CP bottom voltage with respect to the CP top voltage is due to positive charge accumulation on the CP bottom electrode, as has been discussed in our previous work.[35)]

Interesting feature of the voltage waveform is observed at the CP bottom electrode. After turning off the VHF power, sharp increase of the CP bottom voltage up to ~120 V is followed by slow voltage decrease. Furthermore, when the VHF power is on, sharp decrease of the CP bottom voltage is followed by slight voltage increase. Different behavior of the V_{AVE}^{BTM} from the V_{AVE}^{TOP} suggests the V_{AVE}^{BTM} is influenced not only by the V_{AVE}^{TOP} but also discharging and charging of the accumulated charge on the bottom electrode.

To understand the mechanism how the V_{AVE}^{BTM} is determined, VHF power is varied and the V_{AVE}^{BTM} at a timing just before the pulse is turned off (t=0.5 ms in Fig. 3) are plotted as a function of the V_{AVE}^{TOP} for ARs of 12, 30 and 50. (Fig. 4). To ease to understand the voltage difference between top and bottom voltages of the CP, the V_{AVE}^{TOP} is also indicated by broken line. The V_{AVE}^{BTM} is always less than ~30 V irrespective of power or AR. This means that the V_{AVE}^{BTM} cannot exceed the plasma potential because ions from the plasma is retarded by the potential of the CP bottom. It is also shown that the voltage difference between the CP top and bottom ($\Delta V_{AVE}=V_{AVE}^{BTM} - V_{AVE}^{TOP}$) increases with increasing the AR at higher CP top voltages.

To give an insight into the behavior of the accumulated charge on the CP bottom electrode, accumulated charge density on the CP bottom electrode

(σ_B) at a timing of just before turning off the pulse (t=0.5 ms in Fig. 3) is analyzed based on the procedure mentioned in chapter 2. Figure 5 shows accumulated charge density on the CP bottom (σ_B) as a function of the V_{AVE}^{TOP} for ARs of 12, 30 and 50. Increase of the positive charge accumulation is seen for ARs of 30 and 50. In the case of AR=12, however, accumulated positive charge shows its peak at V_{AVE}^{TOP} ~100 V, and gradually decreases with the V_{AVE}^{TOP}. Another interesting feature is charge density for AR=50 at low V_{AVE}^{TOP}, where charge density is much lower than those for AR=12 and 30. The mechanisms of these dependencies will be discussed later.

Next, time dependence of accumulated charge is investigated. Figure 6 shows temporal variations of the σ_B at AR=50, changing the VHF power from 50 to 400 W. As has been shown in Fig. 5, σ_B increases with the VHF power. In addition, charge-up and discharge of the σ_B are clearly observed during the pulse-on and -off phases, respectively. Charge decrease is very slow in the pulse-off phase and charging-up is very quick in the pulse-on phase, except for the 50 W VHF power case. Very low charging currents at low VHF powers indicate that ions with low kinetic energies from the plasma cannot reach the CP bottom due to very high AR. This is also confirmed by the fact that such low charge accumulation rate at low VHF powers is not observed for ARs of 12 and 30 (not shown here). From these results, we can conclude that very low σ_B only in the case of low VHF powers and high AR of 50 is caused by low charging current during the pulse-on phase that is comparable with the discharge current during the pulse-off phase.

To understand the charge accumulation behavior, an equivalent circuit model is proposed (Fig. 7). In the figure, C_{CP} and C_{ALM} are effective capacitances of the CP and the alumina plate, respectively, and their values have been already known as 48 pF and 22 pF, respectively, from our previous work.[35] C_A (6.6 pF) and R_A (100 MΩ) are stray capacitance and input resistance of the HVP, respectively. The CP used in this study is made of lead glass and has some leak conductance. Its resistance is considered as R_{CP}. A current source shown in the figure represents flux of charged particles (ion, electron) from the plasma to the CP bottom through the CP hole. A voltage source on the CP top represents the negative self-bias voltage in the pulse-on phase, and slight positive voltage in the pulse-off afterglow phase. The current from the current source is influenced not only by the plasma density but also by the CP top and the CP bottom voltages, because the high-energy ion current and electron current to the CP bottom are influenced by the retarding and accelerating potential of the CP bottom voltage, respectively. Accordingly, the current from the current source should be considered as net current averaging over ion and electron currents those vary with the VHF phase.

To confirm the validity of this model (especially leak current of the CP), charge decay behavior of Fig. 6 is investigated. Figure 8(a) schematically shows spatial profile of electric potential from the CP top to the powered electrode after the electron temperature is lowered and self-bias voltage disappeared in the pulse-off phase. Voltages of both the CP top and the powered electrode are ~10V and ~0 V from the measurements (not shown

here). Accumulated charge on the CP bottom produces potential peak (V_{AVE}) at the CP bottom. Based on the equivalent circuit model, charge on the CP bottom is accumulated on parallel capacitances of C_{CP}, C_{ALM} and C_A at the voltage of V_{AVE}. Accordingly, current (I_0^{OFF}) flowing out from the CP bottom immediately after turning off the pulse is described as

$$I_0^{OFF} = \frac{R_A + R_{CP}}{R_A \cdot R_{CP}} \Delta V_{AVE} \ , \qquad (1)$$

assuming that the CP top is grounded. Although the CP top voltage is not 0 V at the pulse-off phase due to the existence of the afterglow plasma, the above equation is still valid when the $\Delta V >> V_{AVE}^{TOP}$ at pulse-off phase. Figure 8(b) shows enlarged graph of the time-dependent σ_B at t~0.5 ms. AR and V_{AVE}^{TOP} are 30 and -155 V. After turning off the pulse, the result shows fast decay which is followed by slow decay. Broken curve is best-fitted exponential curve using slow decay data (t >0.8 ms). The difference between the best-fitted curve and the experiment at t=0.5~0.7 ms is due to the electron current flowing from the afterglow plasma to the CP bottom. Solid blue curve shows charge decay by the CP leak supposing no decrease of CP positive charge by afterglow electron current. We have measured time dependent electron density during the pulse-off phase using time-resolved surface wave probe measurement[36]. Measured decay time constant was ~0.1 ms that is comparable to the time-scale of the electron decay time constant in the figure.

Removing the influence of the afterglow electron current, I_0^{OFF} is

obtained from the slope the best-fitted current at t=0.5 ms, as shown in the figure. From the measured I_0^{OFF}, current density J_0^{OFF} is obtained taking account for the thickness (0.3 mm), area (4.9 cm^2) and opening ratio of the CP holes (~60%). Figure 9 shows measured J_0^{OFF} as a function of the ΔV_{AVE}. The current density is almost proportional to the ΔV_{AVE}. The result clearly shows that the resistivity of the CP is almost the same irrespective of the AR. From the slope of Fig. 9, parallel resistance of R_{CP} and R_A are 75 MΩ, and R_{CP} value of 300 MΩ is obtained using R_A value of 100 MΩ. We have measured the CP resistance using a high-resistance probe, changing the CP temperature and almost comparable value has been obtained at CP temperatures of ~70 ºC. In addition, decay time constant of the best-fitted curve in Fig. 8 was almost consistent with the RC time constant based on the equivalent circuit model of Fig. 7.

By removing the CP leakage charge from the time-dependent σ_B during the pulse-off phase (*c.f.*, Fig. 8(b)), we can obtain positive charge cancellation by negatively-charged electron flowing to the CP bottom. Figure 10 shows negative electron charge density accumulated on the CP bottom by the afterglow electron current for ARs of 12, 30 and 50. With the time after turning-off the VHF pulse, electron charge accumulation starts and saturates at t=0.8~0.9 ms, *i.e.*, 0.3~0.4 ms after turning-off the plasma. Increase of the charge accumulation is also observed with higher VHF powers and lower ARs. The result shows that the negative charge accumulation is influenced by the electron transmission probability through the hole and that the probability is determined by the CP bottom voltage

(ΔV_{AVE}) and the AR. In Fig. 5, decrease of the positive charge density is observed at higher V_{AVE}^{TOP}, especially in the case of AR=12. This is partly due to negative charge accumulation during the pulse-off phase at low ARs and higher VHF powers.

Finally, positive charge-up during the pulse-on phase is discussed. Figure 11 shows charging current obtained from the slope of the σ_B at t=0 in Fig. 6. Please note that the horizontal axis is not the ΔV_{AVE} but ΔV_{AVE} at t=0. (ΔV_{AVE} is the voltage difference between the CP TOP and the CP bottom just before turning off the pulse, but ΔV_{AVE} at t=0 is the voltage difference just before starting the CP bottom recharge). In the figure, the leak current through the CP is removed from the measured current, and only the charging current through the hole is shown in the figure. The charging current monotonically increases with the ΔV_{AVE} at t=0 both for AR=30 and 50, and the charging current of AR=50 is smaller than that of AR=30. Charging current density is in order of several μA/cm^2, which is much smaller than the ion current density expected from the plasma density (~mA/cm^2).

4. Conclusion

In conclusion, charge density on the bottom of the high-aspect-ratio (HAR) capillary plate (CP) is quantitatively investigated in a pulse-modulated VHF capacitively-coupled plasma. Based on a carefully calibrated measurement setup, VHF peak-to-peak voltage as well as average voltage on the bottom of the CP was measured. Using an equivalent circuit model, average

voltage on the top of the CP was estimated and charge density on the bottom of the CP (σ_B) was obtained. The charge density on the CP bottom (σ_B) varied depending on the self-bias voltage of the CP top as well as the aspect ratio (AR). Time-dependent σ_B showed charge-up and discharge behavior of the CP bottom in pulse-on and -off phases, respectively. From the equivalent circuit model, it was concluded that the discharge of the accumulated charge from the CP bottom during the pulse-off phase was caused partly by the leakage current flowing through the CP material (lead glass) and partly by electron current in the afterglow plasma.

References

1) W. Tsai, G. Mueller, R. Lindquist, B. Frazier, and V. Vahedi: J. Vac. Sci. Technol. B **14** (1996) 3276.

2) T. Kitajima, Y. Takeo, Z. Lj. Petrović, and T. Makabe: Appl. Phys. Lett. **77** (2000) 489.

3) M. M. Turner and P. Chabert: Phys. Rev. Lett. **96** (2006) 205001.

4) J. Schulze, T. Gans, D. O'Connell, U. Czarnetzki, A. R. Ellingboe and M. M. Turner: J. Phys. D. Appl. Phys. **40** (2007) 7008.

5) T. Shimada, T. Yagisawa and T. Makabe: Jpn. J. Appl. Phys. **45** (2006) 8876.

6) T. Makabe and T. Yagisawa: Plasma Sources Sci. Technol.**18** (2009) 014016.

7) H. Jansen, H. Gardeniers, M. De Boer, M. Elwenspoek and J. Fluitman: J. Micromech. Microeng. **6** (1996) 14.

8) H. Abe, M. Yoneda and N. Fujiwara: Jpn. J. Appl. Phys. **47** (2008) 1435.

9) B. Wu, A. Kumar and S. Pamarthy: J. Appl. Phys.**108** (2010) 051101.

10) T. Iwase, Y. Kamaji, S. Y. Kang, K. Koga, N. Kuboi, M. Nakamura, N. Negishi, T. Nozaki, S. Nunomura, D. Ogawa, M. Omura, T. Shimizu, K. Shinoda, Y. Sonoda, H. Suzuki, K. Takahashi, T. Tsutsumi, K. Yoshikawa, T. Ishijima and K. Ishikawa: Jpn. J. Appl. Phys. **58** (2019) SE0802.

11) J. P. Gambino, S. A. Adderly and J. U. Knickerbocker: Microelectron. Eng. **135** (2015) 73.

12) N. Fujiwara, T. Maruyama and M. Yoneda: Jpn. J. Appl. Phys. **34** (1995) 2095.

13) N. Fujiwara, T. Maruyama and M. Yoneda: Jpn. J. Appl. Phys. **35** (1996) 2450.

14) T. Kinoshita, M. Hane and J. P. McVittie: J. Vac. Sci. Technol. **14** (1996) 560.

15) G. S. Hwang and K. P. Giapis: J. Appl. Phys. **81** (1997) 3433.

16) G. S. Hwang and K. P. Giapis: J. Vac. Sci. Technol. **15** (1997) 1741.

17) V. Ishchuk, B. E. Volland, M. Hauguth, M. Cooke and I. W. Rangelow: J. Appl. Phys. **112** (2012) 084308.

18) K. Yonekura, M. Kiritani, S. Sakamori, T. Yokoi, N. Fujiwara and H. Miyatake: Jap. J. Appl. Phys. **37** (1998) 2314.

19) T. Shimmura, S. Soda, S. Samukawa, M. Koyanagi and K. Hane: J. Vac. Sci. Technol. **22** (2004) 533.

20) T. Shimmura, S. Soda, S. Samukawa, M. Koyanagi and K. Hane: J. Vac. Sci. Technol. **20** (2002) 2346.

21) T. Shimmura, Y. Suzuki, S. Soda, S. Samukawa, M. Koyanagi and K. Hane: J. Vac. Sci. Technol. **22** (2004) 433.

22) S. J. Kim, H. J. Lee, G. Y. Yeom and J. L. Koo: Jap. J. Appl. Phys. **43** (2004) 7261.

23) S. Samukawa: Jpn. J. Appl. Phys. **45** (2006) 2395.

24) J. C. Arnold and H. H. Sawin: J. Appl. Phys. **70** (1991) 5314.

25) A. P. Mahorowala and H. H. Sawin: J. Vac. Sci. Technol. **20** (2002) 1084.

26) M. Watanabe, D. M. Shaw and G. J. Collins: Appl. Phys. Lett. **79** (2001) 2698.

27) T. Shibayama, H. Shindo and Y. Horiike: Plasma Sources Sci. Technol. **5** (1996) 254.

28) H. Ohtake and S. Samukawa: J. Vac. Sci. Technol. **20** (2002) 1026.

29) S. Samukawa, and T. Mieno: Plasma Sources Sci. Technol. **5** (1996) 132.

30) C. J. Choi, O. S. Kwon and Y. S. Seol: Jpn. J. Appl. Phys. **37** (1998) 6894.

31) J. H. Kim, C. J. Kang, T. H. Ahn and J. T. Moon: Thin Solid Films **345** (1999) 124.

32) K. Kurihara and M. Sekine: Jpn. J. Appl. Phys. **39** (2000) 1369.

33) H. Ohtake, B. Jinnai, Y. Suzuki, S. Soda, T. Shimmura and S. Samukawa: J. Vac. Sci. Technol. **24** (2006) 2172.

34) N. Negishi, M. Miyake, K. Yokogawa, M. Oyama, T. Kanekiyo and M. Izawa, J. Vac. Sci. Technol. **35** (2017) 051205.

35) M. Moriyama, N. Nakahara, A. Mitsuya, H. Suzuki, K. Kurihara, D. Iino, H. Fukumizu and H. Toyoda, Jpn. J. Appl. Phys., **59** (2020) SJJB03.

36) H. Kokura, K. Nakamura, I. P. Ghanashev and H. Sugai, Jpn. J. Appl. Phys., **38** (1999) 5262.

Figure Captions

Fig. 1. Schematic of capillary plate setting on the powered electrode.

Fig. 2. Typical waveform of CP bottom electrode in pulse-modulated VHF Ar plasma. AR is 30. VHF power is 200 W.

Fig. 3. Average voltage of CP bottom (V_{AVE}^{BTM}) after removing 40 MHz voltage oscillation of Fig. 2 and estimated average CP top voltage (V_{AVE}^{TOP}) evaluated from V_{PP}^{BTM}.

Fig. 4. V_{AVE}^{BTM} at t=0.5 ms (just before turning off the pulse) as a function of the V_{AVE}^{TOP}.

Fig. 5. Charge density on the CP bottom at t=0.5 ms (just before turning off the pulse) as a function of the V_{AVE}^{TOP}.

Fig. 6. Time dependent charge density on the CP bottom at different VHF powers from 50 to 400 W. AR of CP is 50.

Fig. 7. Schematic structure in the vicinity the CP and equivalent circuit model.

Fig. 8. (a) Schematic of potential profile at pulse-off phase. (b) Decay

of CP bottom charge in pulse-off phase. AR and V_{AVE}^{TOP} are 30 and 254Vm respectively. Small dots are experimental results. Broken curve shows best-fitted exponential curve using experimental data of t=0.7~1.0 ms.

Fig. 9. Current density at t=0.5 ms (just after turning off the pulse) as a function of the voltage difference between CP top and bottom.

Fig. 10. Charge density of electron accumulation on the CP bottom during the pulse-off phase for ARs of (a) 12, (b) 30 and (c) 50.

Fig. 11. Charging current at t=0 (just after turning on the pulse) as a function of the voltage difference between CP top and bottom at t=0. CPs with ARs of 30 and 50 are used.

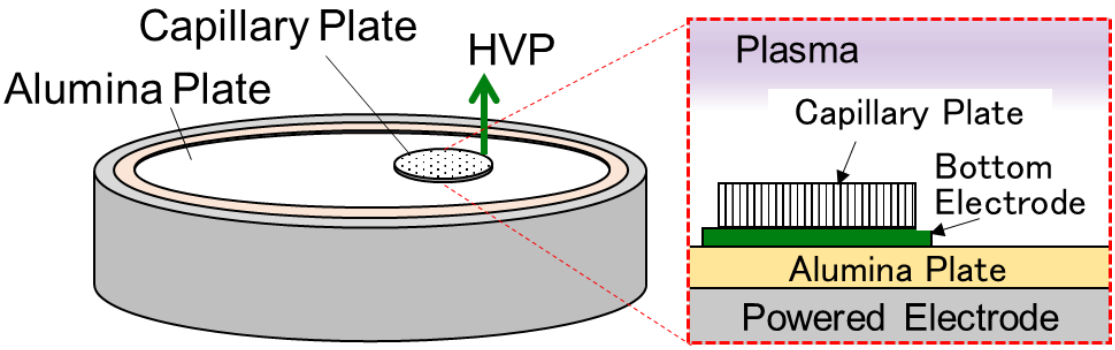

Fig. 1. Schematic of capillary plate setting on the powered electrode.

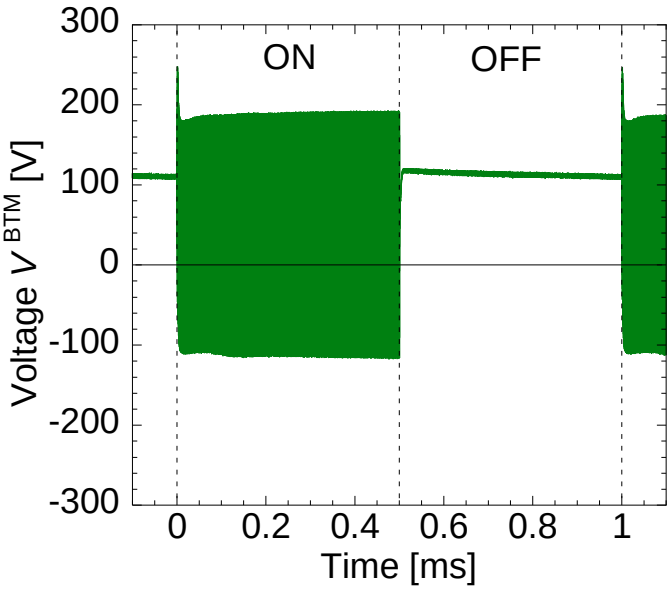

Fig. 2. Typical waveform of CP bottom electrode in pulse-modulated VHF Ar plasma. AR is 30. VHF power is 200 W.

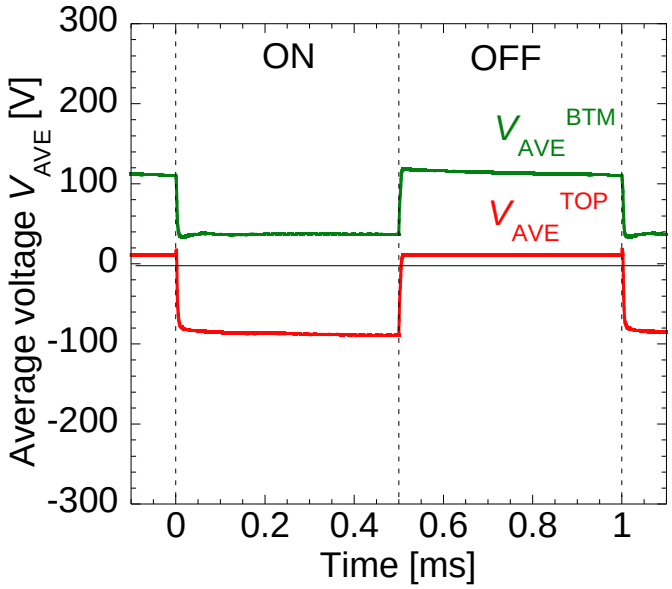

Fig. 3. Average voltage of CP bottom (V_{AVE}^{BTM}) after removing 40 MHz voltage oscillation of Fig. 2 and estimated average CP top voltage (V_{AVE}^{TOP}) evaluated from V_{PP}^{BTM}.

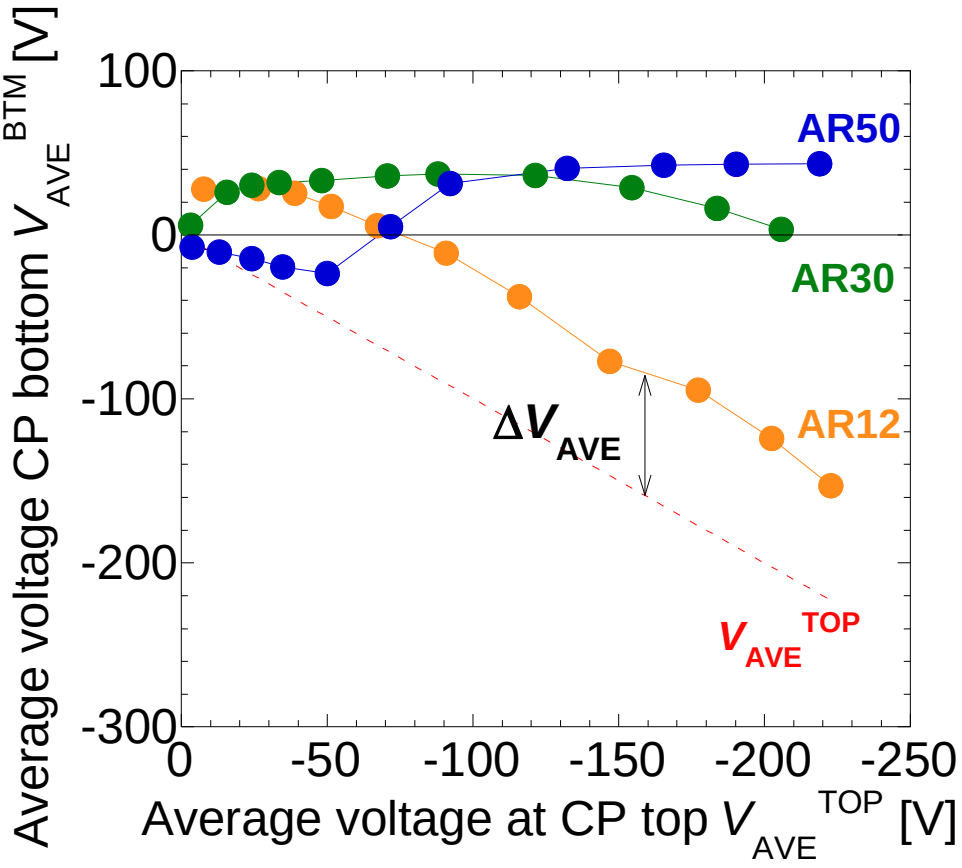

Fig. 4. V_{AVE}^{BTM} at t=0.5 ms (just before turning off the pulse) as a function of the V_{AVE}^{TOP}.

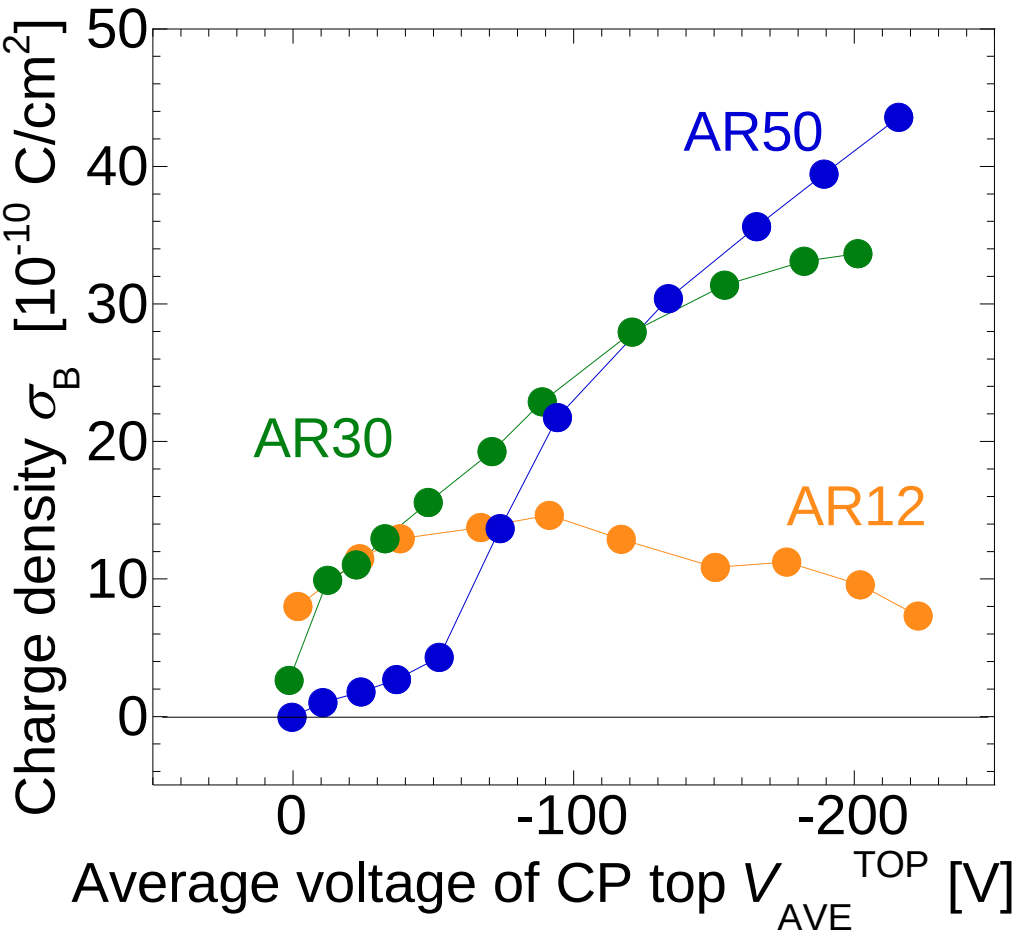

Fig. 5. Charge density on the CP bottom at t=0.5 ms (just before turning off the pulse) as a function of the V_{AVE}^{TOP}.

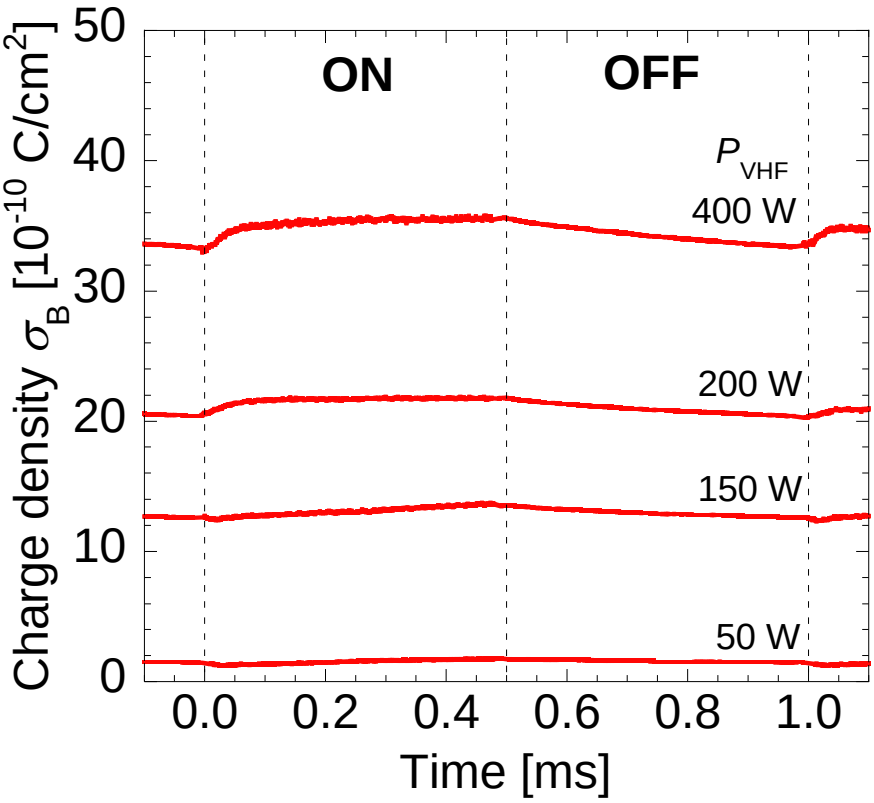

Fig. 6. Time dependent charge density on the CP bottom at different VHF powers from 50 to 400 W. AR of CP is 50.

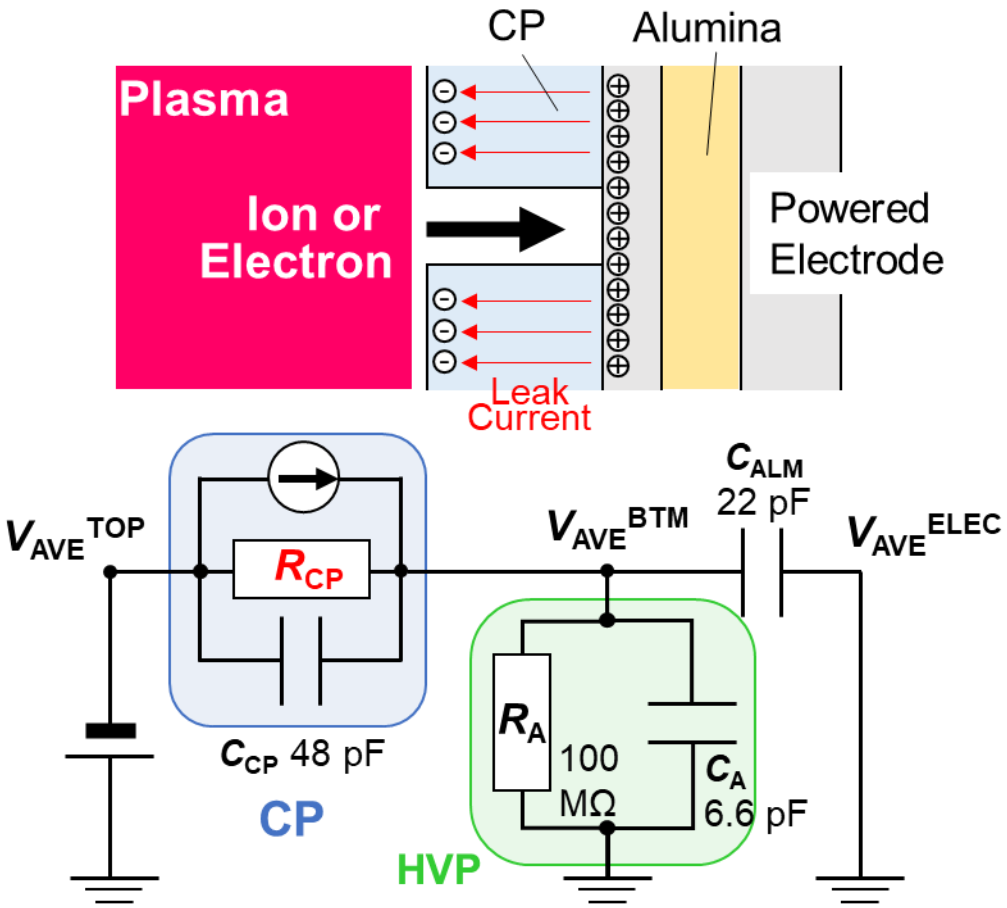

Fig. 7. Schematic structure in the vicinity the CP and equivalent circuit model.

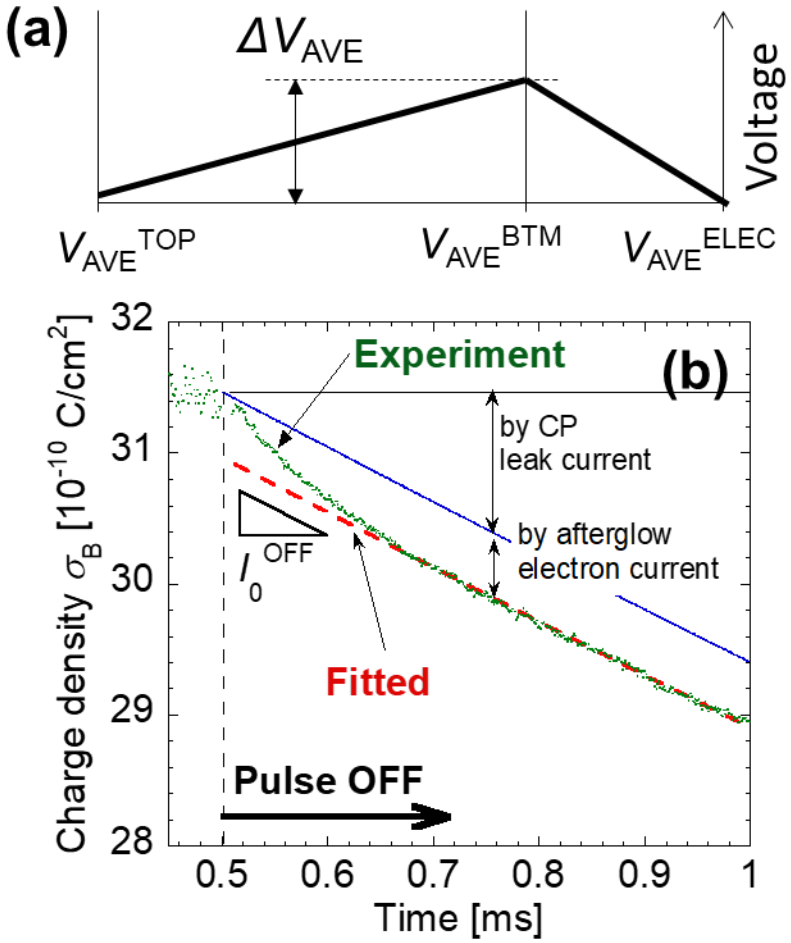

Fig. 8. (a) Schematic of potential profile at pulse-off phase. (b) Decay of CP bottom charge in pulse-off phase. AR and V_{AVE}^{TOP} are 30 and 254V, respectively. Small dots are experimental results. Broken curve shows best-fitted exponential curve using experimental data of t=0.7~1.0 ms.

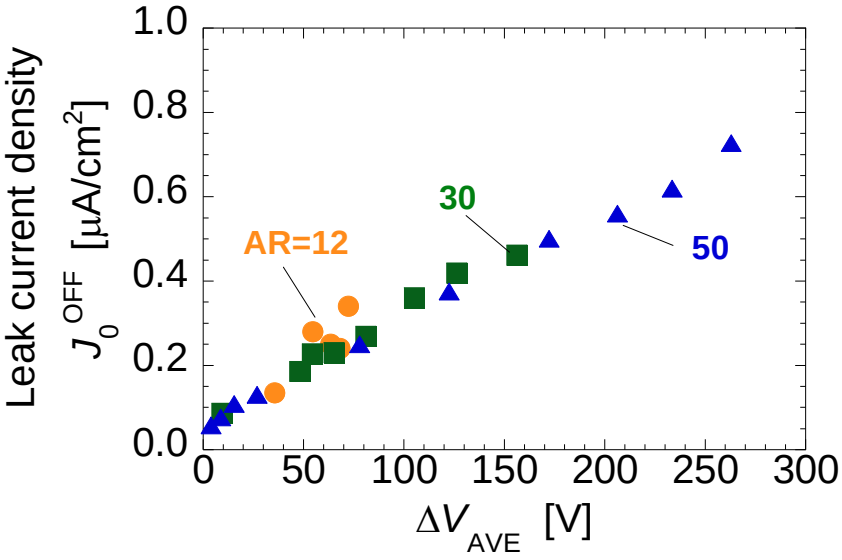

Fig. 9. Current density at t=0.5 ms (just after turning off the pulse) as a function of the voltage difference between CP top and bottom.

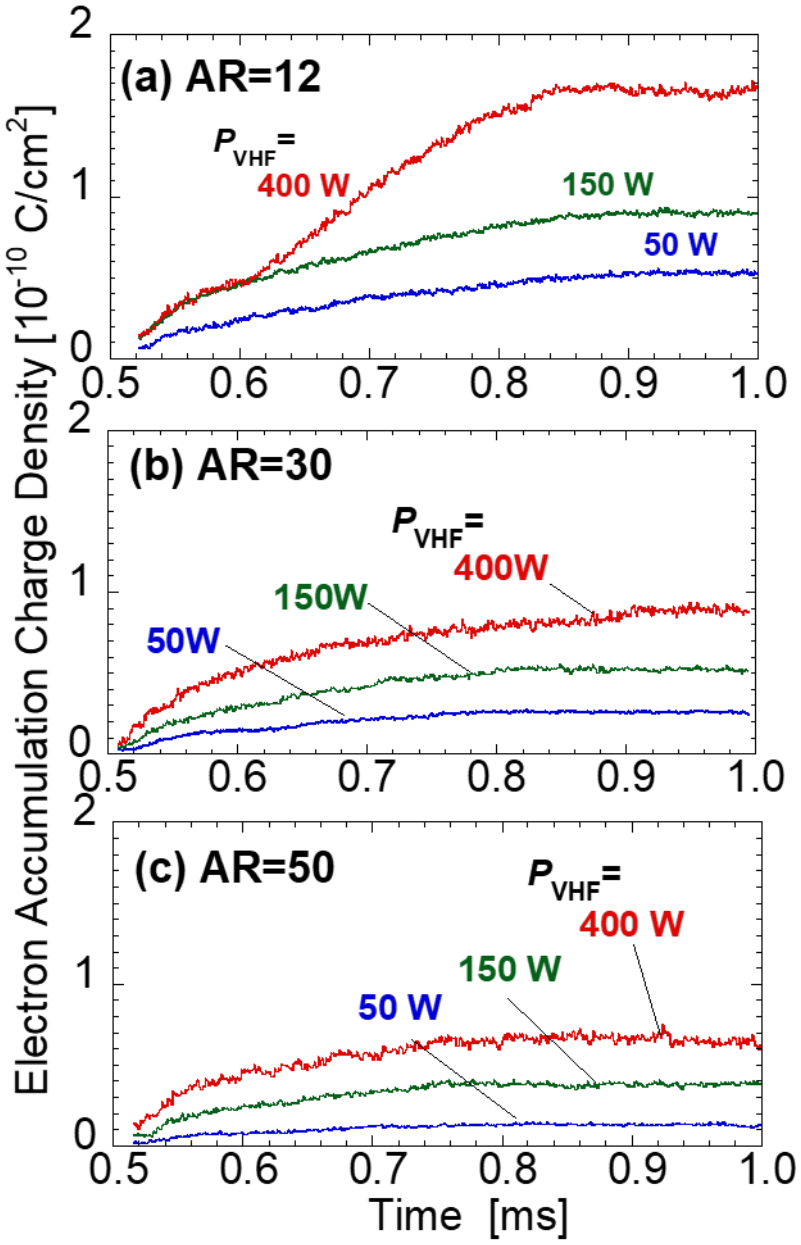

Fig. 10. Charge density of electron accumulation on the CP bottom during the pulse-off phase for ARs of (a) 12, (b) 30 and (c) 50.

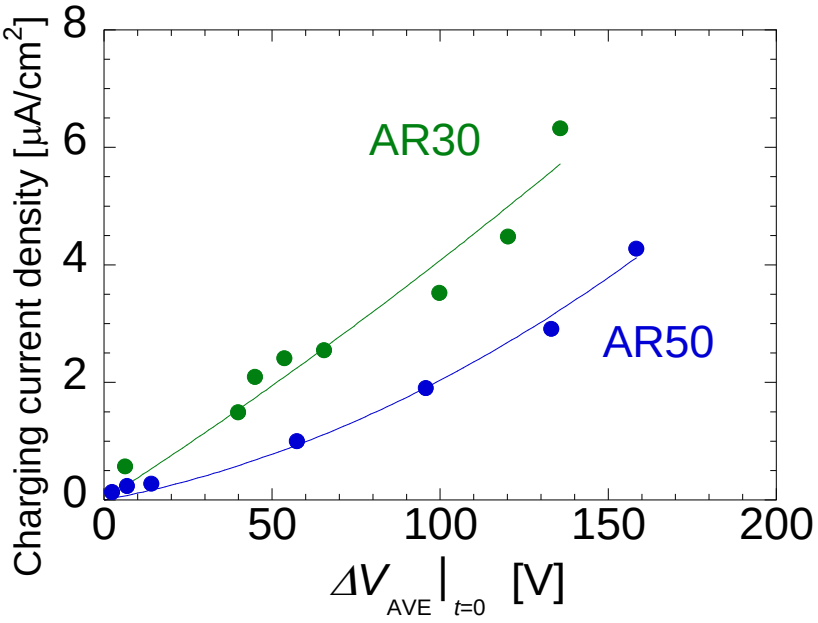

Fig. 11. Charging current at t=0 (just after turning on the pulse) as a function of the voltage difference between CP top and bottom at t=0. CPs with ARs of 30 and 50 are used.